

Microstructure and Mechanical Behavior of Welded and Heat-Treated AISI 1020 Steel

Nitesh Sharma¹ · Ojas Sharma¹ · Saurabh Dewangan¹ 

Received: 8 February 2024 / Accepted: 26 February 2024
© The Institution of Engineers (India) 2024

Abstract Post weld heat treatment methods are widely adopted to improve the mechanical properties of AISI 1020 steel. AISI 1020 is a low-carbon grade of steel which is usually ductile and strong. It shows a fair weldability under all types of fusion welding techniques. This work deals with the microstructure and mechanical property analysis of AISI 1020 steel plates which were first welded by ‘shielded metal arc welding (SMAW)’ and then heat treated. During heat treatment, heating temperature and holding time were kept same for all the samples while the rate of cooling was changed for every welded sample. One welded plate was kept in ‘as received or original’ condition so that a comparative assessment can be done on its behalf. The microstructural appearance was found in good relationship with the tensile strength and hardness of the samples. A huge alteration of microstructure was reported in the study. The sand cooled sample, due to possessing coarse $\alpha + \text{Fe}_3\text{C}$, imparts 7% lesser hardness and 85% higher tensile strength in comparison to ‘as received’ sample. The Also, XRD analysis was carried out to check the phases present in each type of sample. The XRD peaks of welded joint of each plate contains two planes of Fe i.e., α (110) and α (200). This means no defects or oxide formation were recorded after heat treatment.

Keywords SMAW · AISI 1020 · Optical microscopy · XRD · Strength · Hardness

Introduction

AISI 1020 is highly demanded category of low carbon steel which imparts nearly 420 MPa of tensile strength, 120 J of toughness, and 123 BHN of hardness. In addition to that, it has very good weldability and formability [1]. In case of arc welding, a sudden local melting and solidification occurs which makes the pearlite finer in the welded region. Also, there is always a possibility of formation of residual stresses in the HAZ [2]. To avoid these issues, the heat treatment after welding is usually adopted. Heating the samples till austenitic region, holding them for a certain period and cooling into a desired rate can provide a substantial change in microstructure and thereby into the mechanical properties [3]. Annealing is the well adopted heat treatment method in the industries to avoid residual stress and to provide adequate toughness and ductility to the steel sample [4, 5]. Similarly, other forms of heat treatment like normalizing, quenching, stress relieving, process annealing, etc. are adopted to make the steel useful for a particular application [6]. Some of the recent research works are summarized here. After a brief heat treatment of SAF 2507 steel, a considerable increment in austenite was reported in the welded region. The sample which was treated at the temperature range of 1080 °C had shown the highest toughness [7]. The laser welding was performed on 301LN steel without the application of filler metal. The reversion treatment was done post welding. The grains at the welded zone were mainly coarse and columnar. The reversion treatment had increased the elongation of the welded joint in comparison to the temper-rolled samples [8]. The HSLA-80 steel was undergone through various post

✉ Saurabh Dewangan
saurabh22490@gmail.com

Nitesh Sharma
nwr8023@gmail.com

Ojas Sharma
sharmaojas124@gmail.com

¹ Department of Mechanical Engineering, Manipal University
Jaipur, Jaipur, Rajasthan 303007, India

weld heat treatment methods. Based on impact test results, it was found that the HAZ was stronger and tougher than the welded zone [9]. It was observed by the fatigue test that the fine grains of the HAZ substantially restricts the crack growth during the test [10]. T91 steel, Cr & Mo based steel, was tested after heat treatment. The longer holding time was found favorable for a better toughness. It is because of the formation of fine martensitic under tempered condition. Also, the soaking period of 2 h had successfully increased the hardness to an optimum level [11]. During the study of welded P92 steel, the ‘as welded’ sample was found with heterogeneous microstructural appearance. The post weld treatment had removed the δ ferrite patches and thereby the hardness range had also changed [12]. The dissimilar joint between A537CL1 and AISI A321 steels has been processed through heat treatment. The treatment temperature of 620 °C was noted as highly relevant for removing residual stresses [13]. The welded joint between 13 and 8 Mo steel and maraging steel had shown a considerable improvement in tensile strength and elongation [14]. The laser welded joint between 2205DSS and Q235 was heat treatment at three different temperature levels. The base metal zone of Q235 showed the fastest diffusion of carbon atoms [15]. The NiTi and SS304 joint shows cracks usually in laser-welded condition. These cracks may be avoided by adding Ni. A work in this direction reported the formation of Ni₃Ti after the temperature rise of post weld heat treated condition. This phenomenon has significantly increased the hardness, which was measured by Vickers hardness tester [16]. The post welded stainless-steel plates, i.e., AISI304L and AISI430, had shown a considerable improvement in mechanical properties and corrosion resistance [17]. In similar manner, other steels like pressure vessel steel [18], grade 91 steel [19], T-250 maraging steel [20], T-91 steel [21], and S690 high strength steels were welded and tested to get the most satisfactory results by various heat treatments. It has been noted that the spaces between lamella of undeformed pearlite can affect the proof strength of the metal. The ferrite content of interstitial-free iron was found with higher yield than the ferrite in the pearlite [22]. The bainite and martensite mixed extremely high strength micro-alloyed steel is being considered for various structural use and automobile applications [23, 24]. Another approach for fabrication of high-strength steel is by using rolling at upper critical temperature followed by thermomechanical process and air cooling. The processed metal was then quenched, partitioned and partial austenitized at 800 °C. This complete process was capable to provide high tensile strength, elasticity, and low yield ratio [25].

In this direction of research, the current work is dealing with AISI 1020 steel for the post weld heat treatment analysis. This work is an extension of the work published by [26]. Four different ways of cooling have been adopted to get the

variation in microstructure and mechanical properties. In addition, these plates were tested under XRD to check any variation in phases present in the welded zone.

Experimental Work

As discussed in [26], AISI 1020 steel plates of dimension 100×50×5 mm was considered as experimental material in this work. A total of 10 nos. of plates were collected to form five pairs of welded joints. SMAW was used as a welding technique in this work. The yield parameters of welding in each category were kept same, i.e., 50 V and 180 A. The cellulose flux coated filler electrode of E6010 was used during welding. Its diameter was 2 mm. The first welded plate was considered as ‘original’ plate as it was not undergone through any heat treatment process whereas other four plates were heated at a temperature level of 950 °C for a soaking time of 1.5 h. This temperature is sufficient for proper conversion of room temperature ferrite + cementite into pure austenite. After a certain period of heating, these plates were removed out of the furnace and cooled in four different media like chilled water, mustered oil, building sand, and atmospheric air at ambient temperature. These plates were allowed to cool until the room temperature in the particular cooling media. The heat treating and cooling work can be understood by the outline given in Fig. 1. Five samples have been named as 1, 2, 3, 4, & 5. Sample 1 is in original condition. Sample 2 and sample 3 are water and oil quenched respectively. Sample 4 is sand cooled whereas sample 5 was named to air cooled sample. Two destructive tests have been carried out by taking all the five welded plates. First, the tensile test by using the ‘universal testing machine’ and second, the hardness test on Rockwell hardness tester. The tensile testing requires a specific shape of specimens as designated by ASTM-E8. These specimens were cut-off by the ‘electric discharge machining’. In these specimens, the cross-sectional area of the mid-portion, nearly 32 mm long, is made smaller than the grip section. During the tensile test, the upper jaw was moved by a strain rate of 0.001 s⁻¹. It has been seen that all the welded specimens were broken through the welded zone (Fig. 2a). The Rockwell hardness test, in B scale, was done on the smooth cross-sectional surfaces on each plate. A number of indentations was done on each welded plate starting from left to right side so that three zones BM, HAZ, and WZ can be covered through the hardness test. The microstructural test was carried out through an optical microscope. For that, the cross-sectional surfaces of each plate were super-finished by using a polishing machine (Fig. 2b). Five different grades of abrasive papers, medium to very fine, were utilized for finishing purpose. The finished surfaces were etched by Nital solution (100 ml ethanol + 4 ml nitric acid). The samples

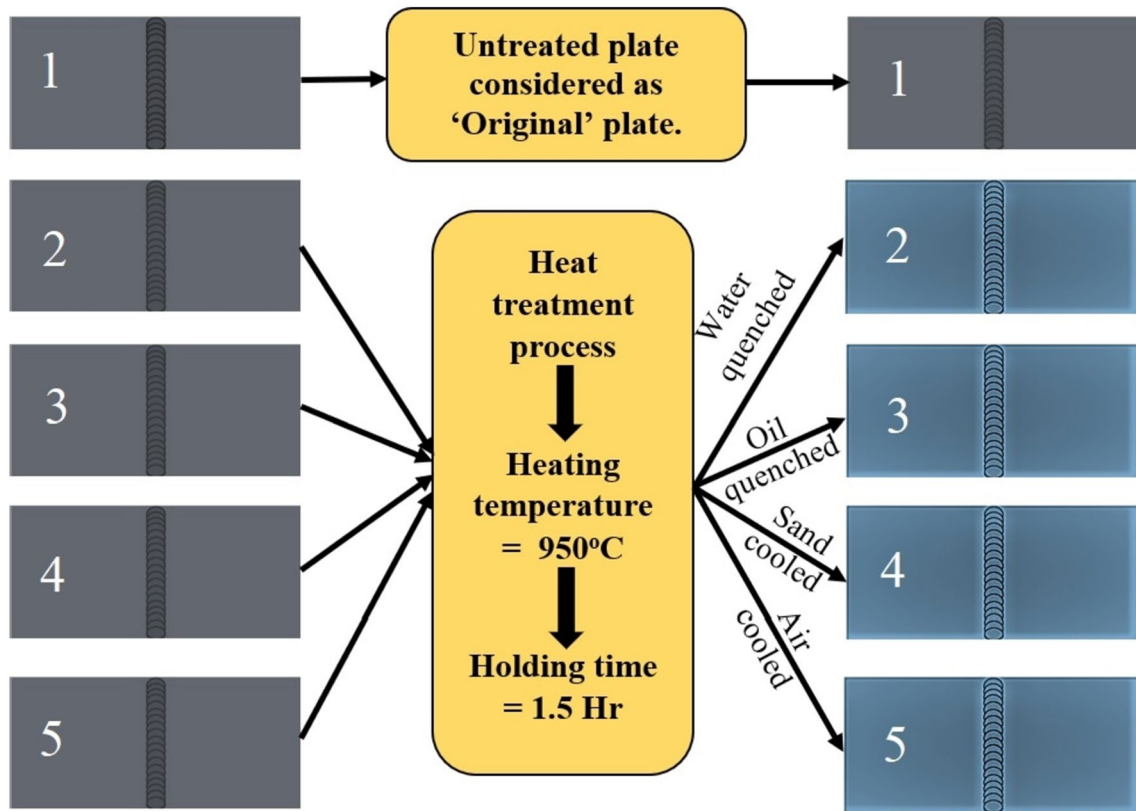


Fig. 1 Process of heat treatment followed during the experimental work

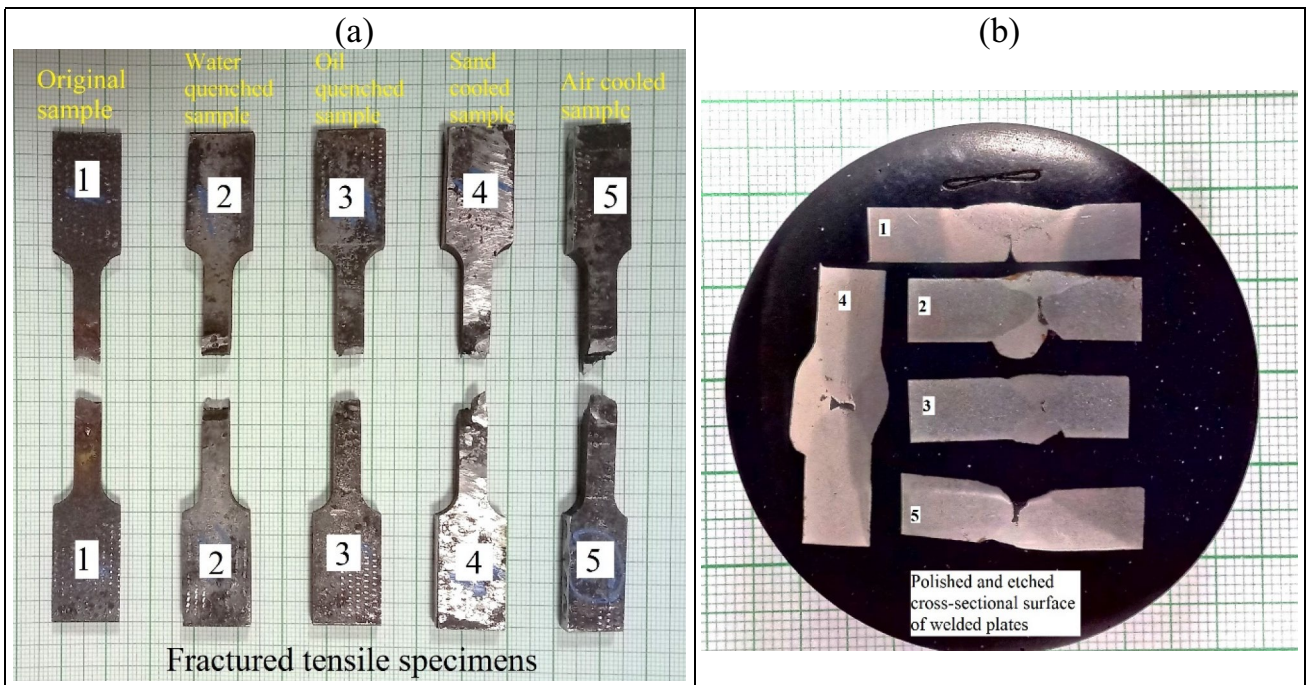


Fig. 2 a Used specimens in tensile test; b Samples for microscopic observation

were dipped into the solution for 8–10 s and then rubbed by cotton prior to microscopic observation. A small portion near the welded joint was cut from each plate for conducting XRD analysis.

Result Analysis

For each welded plate, four microstructural images were captured. One image was captured at 200X magnification at HAZ where a boundary is clearly visible between BM and WZ. Three other images were captured at 1000X magnification at three different zones- BM, HAZ, and WZ. The heat treatment methods have substantially changed the grain structure of each plate. The images of sample 1 are given in Fig. 3. The HAZ image at 200X was captured near the fusion boundary where microstructural changes occurred. The exact BM has been shown at 1000X magnification in which ferrite and pearlite regions can be easily recognized. The ferrite and pearlite are mainly coarse in appearance. Also, a lamellar structure of ferrite and cementite can be seen in the

pearlitic region. As soon as, the observation moves toward the WZ, the pearlite gets elongated over the ferrite zone. It is because of sudden melting and localized cooling of the fusion zone. The microstructure of sample 2 has been shown in Fig. 4. The BM side of the plate has converted into martensite as its presence is very fine like needles. No bright regions are available as proof of ferrite initiation. Also, the pearlite formation is restricted in the BMZ. The boundary area between BMZ and WZ shows a conversion from martensite to pearlite. The pearlite and ferrite growth toward the WZ can be seen in the boundary region. The WZ is containing a mixture of ferrite, pearlite and fine elongated structure of bainite. The alternate lamella of α ferrite and cementite (Fe_3C) can also be observed as a proof of reduction in hardness in comparison to BMZ. Figure 5 discusses the microstructural appearance of oil quenched sample. Like sample 2, it has martensitic grains throughout the BM although some ferritic growth has been started which can be recognized through its bright appearance. The BM-WZ boundary is clearly showing the ferrite growth toward welded region. The WZ consists fairly coarse ferrite and pearlite along with

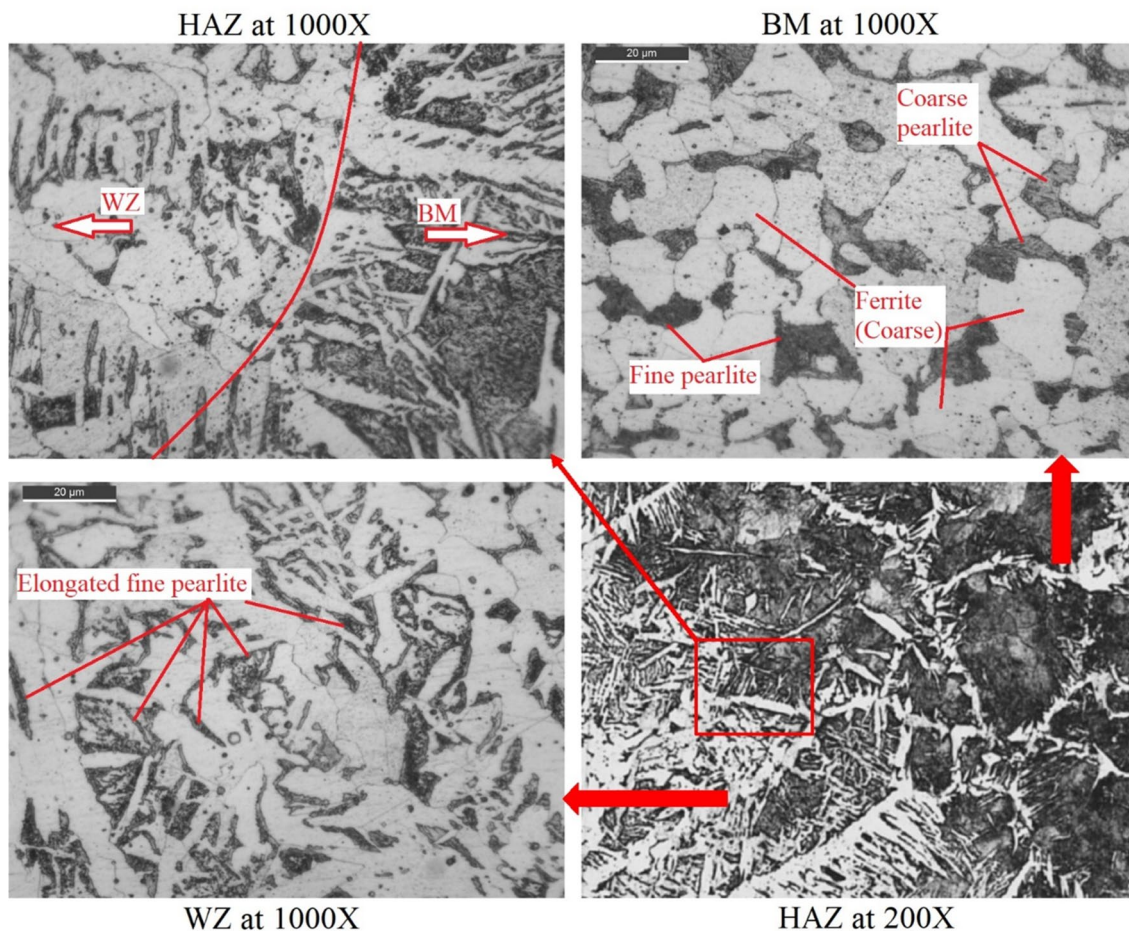


Fig. 3 Microstructure in sample 1 (original sample)

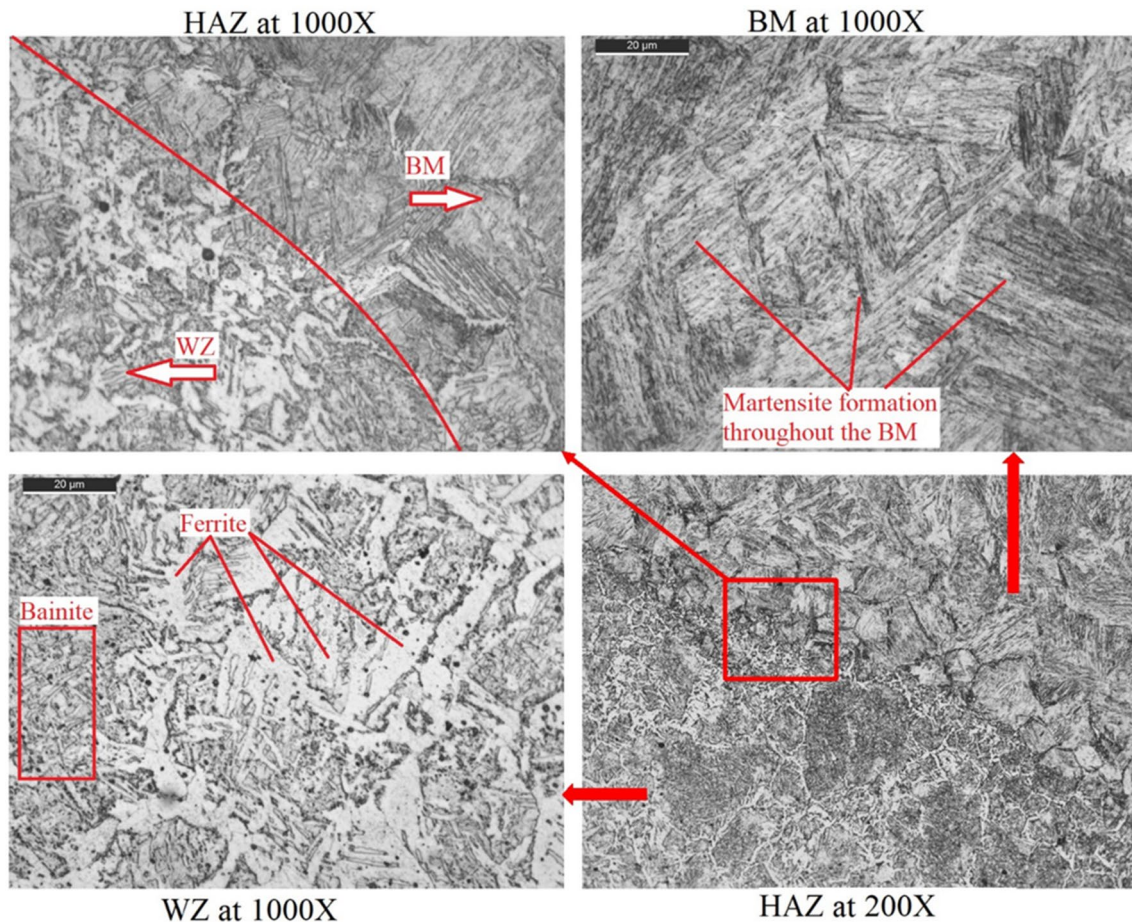


Fig. 4 Microstructure in sample 2

fine bainites. These bainites have made the WZ harder than HAZ. The microstructural images of sample 4 (sand cooled) have been shown in Fig. 6. In comparison to sample 1, 2, and 3, sample 4 is possessing larger grains of ferrite and pearlite. The pearlite is possessing a wide lamella of ferrite and cementite in this case. These coarse grains get elongated and columnar as soon as the BMZ-WZ boundary is crossed. The WZ is showing a dendritic pearlite formation in the sand cooled sample. Hence, the WZ was found harder than the HAZ and BMZ. Sample 5, the air-cooled sample, shows the similar attributes of microstructure as discussed for sample 1. The BM is carrying coarse ferrite and fine pearlite. The lamellar growth of ferrite + cementite is hardly visible in the BMZ even at the 1000X magnification. The fusion boundary is drastically changing the orientation of pearlite from BM to WZ. As soon as the WZ reaches, the pearlite gets coarser (Fig. 7). However, the overall grains structure in the WZ is columnar and dendritic and hence the hardness is higher than the BM zone.

The results of *tensile test* have been compared with the same of original specimen. The tensile test result was

obtained as ultimate tensile stress (UTS) value and maximum elongation (E_m) in the specimen till fracture. A bar chart is shown in Fig. 8 for a comparative assessment of tensile test results. The UTS and E_m in sample 1 were reported as 237 MPa and 1.525 mm respectively. In sample 2, the water quenching phenomenon has reduced the UTS of the specimen up to 208 MPa and that is approximately 12% smaller than the same of sample 1. There is a substantial reduction of 41% in E_m during water quenching. Sample 3 was cooled inside Oil which has shown better UTS than sample 2. Sample 3 is possessing the UTS of 227 MPa that is only 4% lower than the original sample. The elongation induced in the oil quenched sample is nearly 52% larger than water quenched product. Hence, for a better tensile properties oil quenching is preferable over water quenching. The sample 4 has shown the highest of UTS and E_m , i.e., 439 MPa and 1.61 mm respectively. The UTS of sample 4 has increased by 85% with respect to original sample. Fifth sample has shown a very poor performance in terms of UTS. It is 179 MPa in this sample. Also, the E_m value is 0.92 mm. According to Fig. 2b, sample 5 has a large undercut during

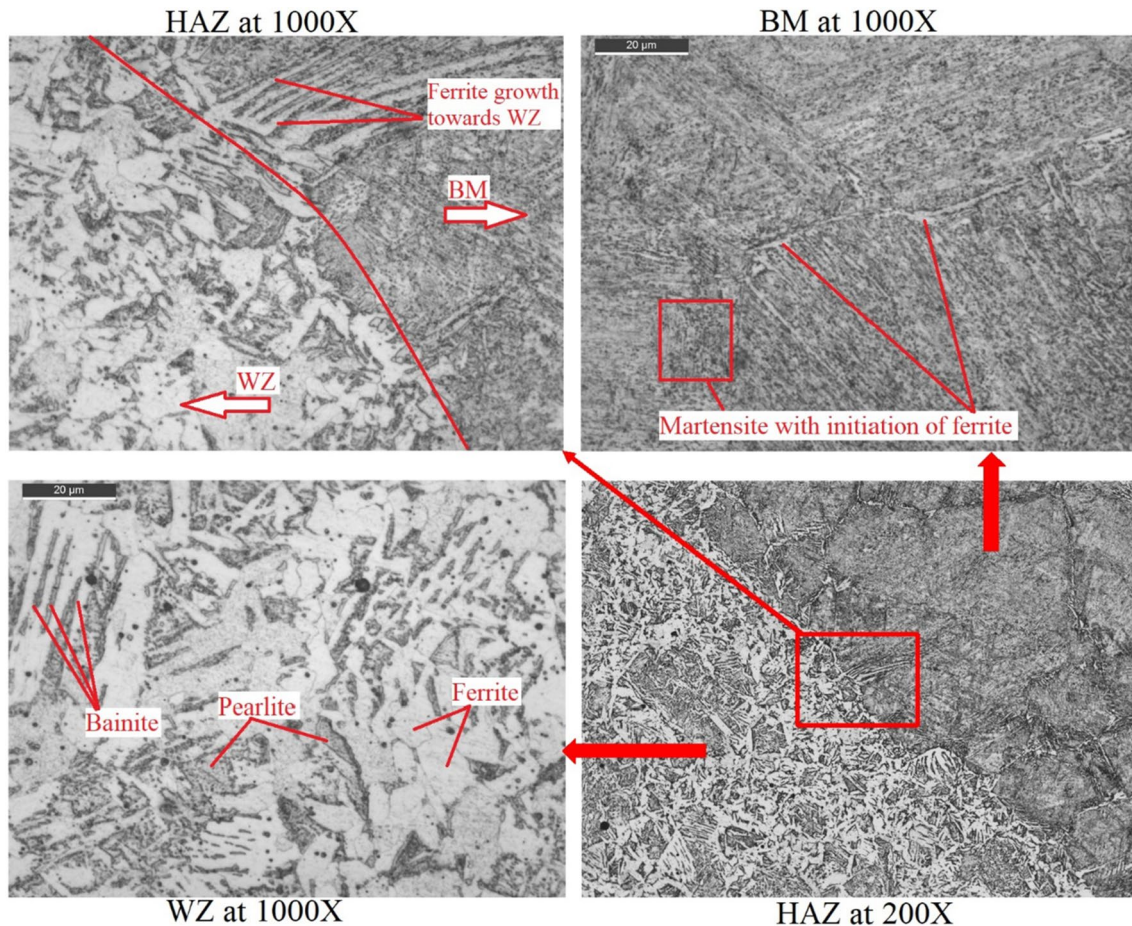


Fig. 5 Microstructure in sample 3

welding and hence proper fusion of base metal did not take place.

The *hardness* of the welded plates was determined by taking total 31 indents on each plate. One indent is on center point of the welded joint and 15 indents on the either side of the joints. The indentation wise hardness values (HRB) are written in Table 1. Negative sign is showing the values on the left side of the joint and positive signs are representing the values at the right side of the plate. The italic values belong to the welded zone whereas the hardness values at the HAZ (both sides) in bold parts. The color-less portions in Table 1 are representing the hardness at the base metal part. The average hardness at three different zones for all the plates are compared by a bar chart given in Fig. 9.

There is an ascending order of hardness from BM to WZ in original sample. The highest hardness was achieved in the WZ due to fine columnar growth of ferrite and pearlite. The water quenching phenomenon has changed the hardness profile of the sample. In this, the BM carries the highest hardness and the HAZ has been found as the least hard. In comparison to the original sample, the BM, HAZ, and WZ

of the water quenched sample carry nearly 14%, 5%, and 5.2% respectively more hardness. The hardness profile of sample 3 is almost similar to sample 2. It means, both the quenching processes have similar effect on the hardness of the samples. All the three zones of the oil quenched sample were found harder as compared to the original sample. The sand cooling process has reduced the hardness of the welded plates at every zone. A decrement of 4%, 6%, and 7% was recorded at the BM, HAZ, and WZ respectively in comparison with the same of sample 1. The hardness pattern in air-cooled sample is similar to that of original sample, although a bit increment in each zone was recorded after air cooling. The air cooling has provided a finer microstructure than in case of original condition.

The *XRD analysis* has been carried out to check various phases present in the welded zone after the heat treatment methods. The XRD image is shown in Fig. 10. The XRD peaks are showing only two planes of iron, i.e., α (110) and α (200) in different intensities. The XRD results are indicating that no defects are present in the welded zone after the heat treatment.

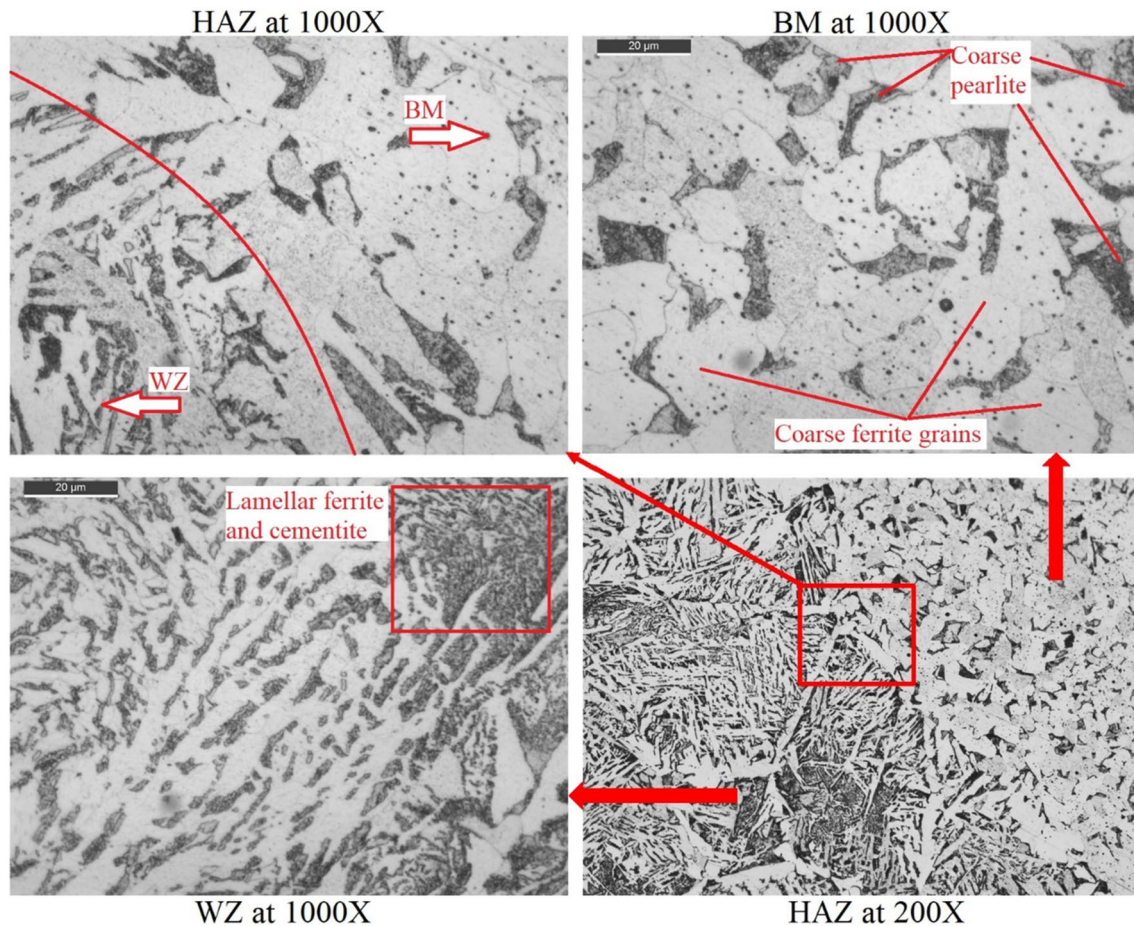


Fig. 6 Microstructure in sample 4

Discussion

It is the type of metal and its composition which finalize the degree of residual stress-leaving. Other than these, the PWHT temperature and the length of soaking time also significantly affect the overall process. For PWHT, a standard protocol is to soak the joint for one hour at room temperature for every 25 mm of thickness; however, in some circumstances, a shorter soak period may be required. PWHT at higher temperatures allows for some aging, precipitation, and/or tempering effects in addition to the reduction and redistribution of residual stresses during the welding process. By lessening the structure's hardness when it is welded, these metallurgical modifications can increase ductility and lower the likelihood of brittle fracture. However, in certain steels, precipitation and aging processes can lead to a decline in the steel's mechanical qualities [27]. PWHT may or may not be required, depending on the material and service requirements. The welding settings and the most likely reason of failure are other factors that impact the requirement for PWHT. PWHT

is required by particular standards for specific grades or thicknesses; nevertheless, when a choice is available, costs and potential drawbacks must be weighed against potential advantages [27, 28]. Because of the high temperatures and lengthy durations required, the energy costs are usually substantial; nevertheless, the expenditures incurred by time delays could be more significant. In order to fully reap the benefits of the process, it is imperative to carefully control the rates of heating/cooling and temperature tolerances [29].

The overall quality of the welded joint depends on the extent of fusion which occurs between the two adjoining edges. Sometimes, due to improper selection of input parameters, the heat input becomes too low to melt the joint surfaces properly. This creates a situation of 'undercut' defect. This defect is highly undesirable as far as strong joint is concerned [30]. In the present work, the problem of undercut was reported in sample 1, 2 and 5. This issue can be avoided by using proper groove and two-sided welding on the plates.

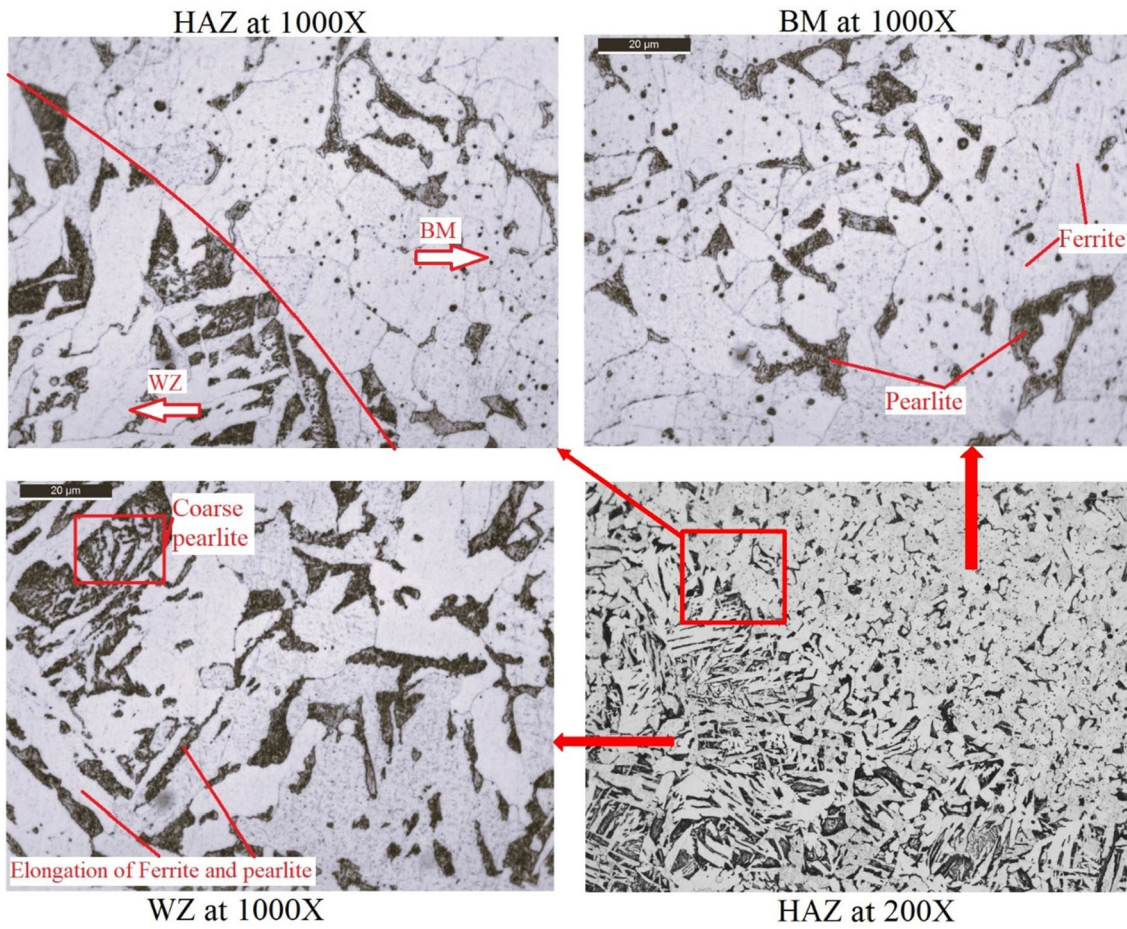


Fig. 7 Microstructure in sample 5

Fig. 8 A comparative analysis of tensile properties in five welded specimens

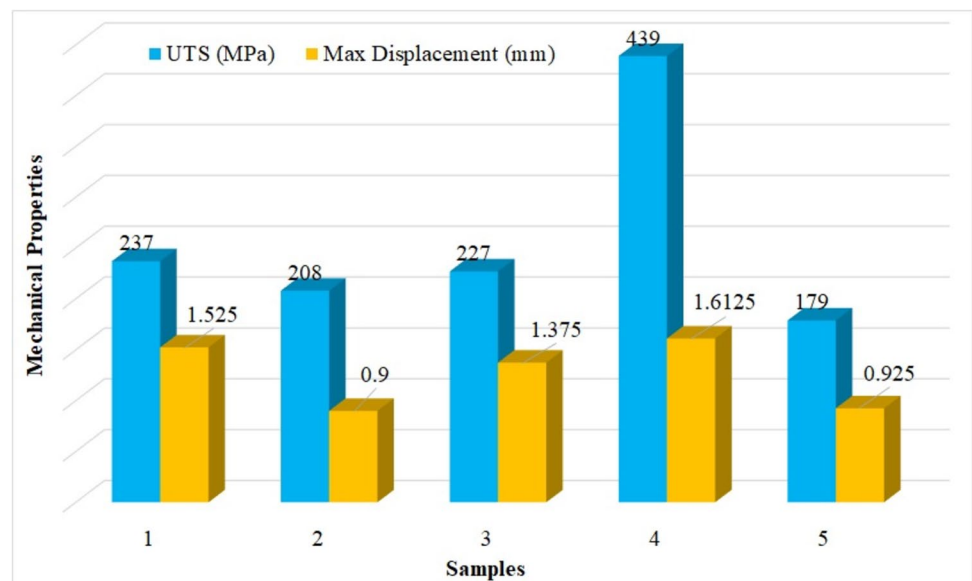


Table 1 Hardness (HRB) at different locations of the plate

Distance from center-point of the WZ (mm)	Sample-1 (Original)	Sample-2 (Water-quenched)	Sample-3 (Oil-quenched)	Sample-4 (Sand cooled)	Sample-5 (Air cooled)
- 30	69	81	82	64	84
- 28	69	82	80	65	65
- 26	68	81	81	66	73
- 24	66	80	79	65	73
- 22	69	83	82	66	72
- 20	68	80	78	67	70
- 18	69	78	76	66	75
- 16	67	76	76	68	72
- 14	70	77	78	68	74
- 12	69	78	76	69	69
- 10	68	76	75	67	66
- 8	72	74	74	67	75
- 6	71	74	74	68	73
- 4	70	76	75	67	75
- 2	75	77	76	69	77
0	74	78	76	69	76
2	74	78	77	68	74
4	73	76	76	66	73
6	72	75	75	67	78
8	73	73	76	65	72
10	70	77	74	66	74
12	68	76	78	67	77
14	69	77	77	68	78
16	70	77	79	66	82
18	67	78	78	68	76
20	66	79	80	69	70
22	69	80	79	67	68
24	69	81	81	65	67
26	67	82	82	63	72
28	68	80	81	64	54
30	68	80	80	62	74

Conclusion

In this work, the effectiveness of post-weld heat treatment has been analyzed by considering AISI 1020 steel plates. After the SMA welding and heat treatment, four samples were cooled into four different ways. The cooling media were selected as: water, oil, sand, and air. Based on the tensile test, hardness test and microstructural attributes, the present work can be concluded as:

1. The microstructural attributes of heat-treated samples are considerably changed as compared with original sample. The base metal of both the quenched plates contains martensite although a small amount of ferritic growth was seen in oil quenched plate. The sand cooled, and air-cooled plates are possessing coarse ferrite but as

far as pearlite appearance is concerned, it is finer in air cooled sample. The BM and WZ boundary show a significant variation in grain structure. In all the samples, a columnar and dendritic growth was noted as soon as the welded zone reached.

2. As far as ultimate tensile stress is concerned, huge increment of 85% was recorded in the UTS of sand cooled sample in comparison to original sample. On the other side, both the quenching media have reduced the UTS. The air-cooled sample has shown the lowest value of UTS in this experimental work.
3. The deformation attained by the specimens till tensile fracture has also been affected by the heat treatment. The maximum elongation was recorded in sand cooled specimen due to possessing coarser ferrite and lamellar pearlite regions.

Fig. 9 Hardness comparison at various zones of five welded plates

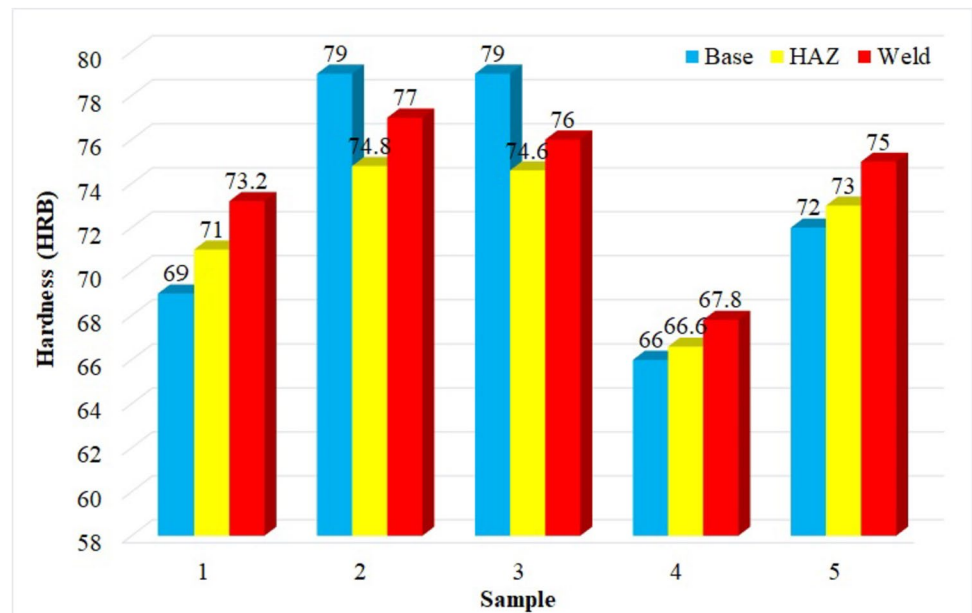
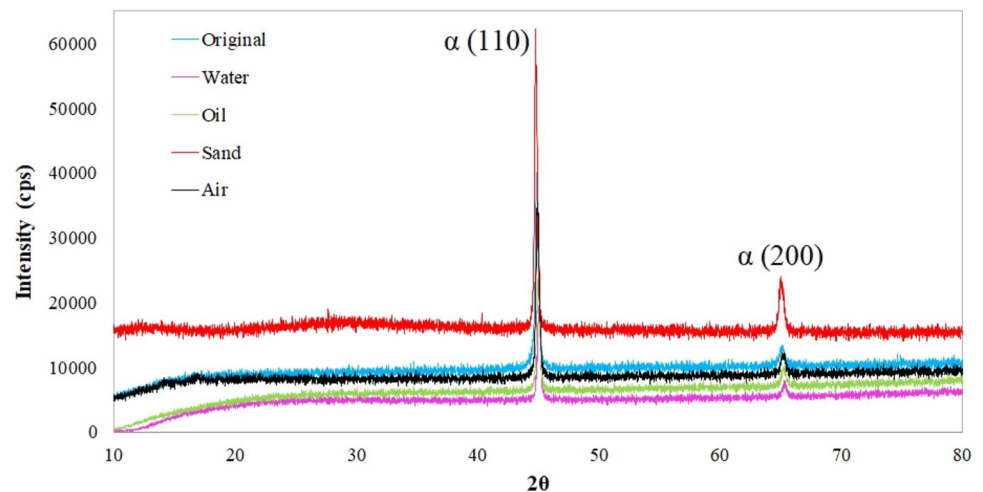


Fig. 10 XRD analysis into welded joint of all the plates



- The hardness pattern in original, sand cooled, and air-cooled sample is similar. In these three samples, the hardness profile is: BM < HAZ < WZ. This pattern has got changed in both the quenched plates. Due to carrying martensitic structure, the BM in both the samples was found harder than other regions. In addition, the WZ in the quenched plates were harder than HAZ due to possessing dendritic growth of ferrite and pearlite.
- The mechanical properties of all the samples, except air cooled sample, were found in good relationship with microstructural appearance. The close observation of the cross-sectional surface of air-cooled sample reveals a significant undercut at the joint which reduced its mechanical properties.
- The XRD peaks of welded zone confirm that no phases other than Fe were present in the steel samples. Hence,

the heat treatment technique has not created any defects like iron oxide.

Author contributions All the authors contributed to the study, conception, and design. NS and OS have performed the experiment and collected the results. SD has written the article. All the authors have read, reviewed, and approved the manuscript before submission.

Funding The authors declare that no funds, grants, or other support were received during the preparation of this manuscript.

Declarations

Conflict of interest The authors have no relevant financial or non-financial interests to disclose.

References

- S. Dewangan, N. Mainwal, M. Khandelwal, P.S. Jadhav, Performance analysis of heat treated AISI 1020 steel samples on the basis of various destructive mechanical testing and microstructural behaviour. *Aust. J. Mech. Eng.* **20**(1), 74–87 (2022). <https://doi.org/10.1080/14484846.2019.1664212>
- J. Verma, R.V. Taiwade, Effect of welding processes and conditions on the microstructure, mechanical properties and corrosion resistance of duplex stainless-steel weldments—a review. *J. Manuf. Process.* **25**, 134–152 (2017). <https://doi.org/10.1016/j.jmapro.2016.11.003>
- S. Dewangan, S.K. Selvaraj, B. Karthikeyan, T.M. Adane, S. Chattopadhyaya, G. Krolczyk, R. Raju, Metallographic investigation on postweld heat-treated 0.21%C-1020 steel plates joined by SMAW method. *Adv. Mater. Sci. Eng.* (2022). <https://doi.org/10.1155/2022/9377591>
- J. T. Black, R. A. Kohser. *DeGarmo's Materials and Processes in Manufacturing* (New York: Wiley) 10th edn (2008)
- J. Kangazian, M. Shamanian, Microstructure and mechanical characterization of Incoloy 825 Ni-based alloy welded to 2507 super duplex stainless steel through dissimilar friction stir welding. *Trans. Nonferrous Met. Soc. China* **29**, 1677–1688 (2019). [https://doi.org/10.1016/S1003-6326\(19\)65074-0](https://doi.org/10.1016/S1003-6326(19)65074-0)
- W.D. Callister, D.G. Rethwisch, *Materials Science and engineering: an introduction*, 10th edn. (John Wiley and Sons, New York, 2018)
- Z. Zhang, H. Zhang, J. Hu, X. Qi, Y. Bian, A. Shen, P. Xu, Y. Zhao, Microstructure evolution and mechanical properties of briefly heat treated SAF 2507 super duplex stainless steel welds. *Constr. Build. Mater.* **168**, 338–345 (2018). <https://doi.org/10.1016/j.conbuildmat.2018.02.143>
- A. Järvenpää, M. Jaskari, M. Keskitalo, K. Mäntyjärvi, P. Karjalainen, Microstructure and mechanical properties of laser-welded high-strength AISI 301LN steel in reversion-treated and temper-rolled conditions. *Proc. Manuf.* **36**, 216–223 (2019). <https://doi.org/10.1016/j.promfg.2019.08.028>
- J.L. de Jesus, V.S. Cândido, A.C. da Silva, F. da Costa Garcia Filho, A.C. Pereira, F.S. da Luz, S.N. Monteiro, Mechanical properties and microstructure of SMAW welded and thermally treated HSLA-80 steel. *J. Mater. Res. Technol.* **7**(4), 598–605 (2018). <https://doi.org/10.1016/j.jmrt.2018.08.007>
- N. Yamaguchi, G. Lemoine, T. Shiozaki, Y. Tamai, Effect of microstructures on notch fatigue properties in ultra-high strength steel sheet welded joint. *Int. J. Fatigue* **129**, 105233 (2019). <https://doi.org/10.1016/j.ijfatigue.2019.105233>
- A. Sharma, D. Kant Verma, S. Kumaran, Effect of post weld heat treatment on microstructure and mechanical properties of Hot Wire GTA welded joints of SA213 T91 steel. *Mater. Today: Proc.* **5**, 8049–8056 (2018). <https://doi.org/10.1016/j.matpr.2017.11.490>
- C. Pandey, M.M. Mahapatra, P. Kumar, J.G. Thakre, N. Saini, Role of evolving microstructure on the mechanical behaviour of P92 steel T welded joint in as-welded and post weld heat treated state. *J. Mater. Process. Tech.* **263**, 241–255 (2019). <https://doi.org/10.1016/j.jmatprotec.2018.08.032>
- B. Sadeghia, H. Sharifi, M. Rafiei, M. Tayebi, Effects of post weld heat treatment on residual stress and mechanical properties of GTAW: the case of joining A537CL1 pressure vessel steel and A321 austenitic stainless steel. *Eng. Fail. Anal.* **94**, 396–406 (2018). <https://doi.org/10.1016/j.engfailanal.2018.08.007>
- C.V.S. Murthy, A. Gopala Krishna, G.M. Reddy, Microstructure and mechanical properties of similar and dissimilar metal gas tungsten constricted arc welds: maraging steel to 13–8 Mo stainless steel. *Defence Technol.* (2019). <https://doi.org/10.1016/j.dt.2018.04.005>
- C. Dua, X. Wanga, C. Luo, Effect of post-weld heat treatment on the microstructure and mechanical properties of the 2205DSS/Q235 laser beam welding joint. *J. Mater. Process. Tech.* **263**, 138–150 (2019). <https://doi.org/10.1016/j.jmatprotec.2018.08.013>
- Y. Chen, S. Sun, T. Zhang, X. Zhou, S. Li, Effects of post-weld heat treatment on the microstructure and mechanical properties of laser-welded NiTi/304SS joint with Ni filler. *Mater. Sci. Eng. A* **13**(771), 138545 (2020). <https://doi.org/10.1016/j.msea.2019.138545>
- S. Ghorbani, R. Ghasemi, R. Ebrahimi-Kahrizsangi, A.H. Najafabadi, Effect of post weld heat treatment (PWHT) on the microstructure, mechanical properties, and corrosion resistance of dissimilar stainless steels. *Mater. Sci. Eng. A* **688**, 470–479 (2017). <https://doi.org/10.1016/j.msea.2017.02.020>
- V.D. Kalyankar, G. Chudasam, Effect of post weld heat treatment on mechanical properties of pressure vessel steels. *Mater. Today: Proc.* **5**, 24675–24684 (2018). <https://doi.org/10.1016/j.matpr.2018.10.265>
- A. Lanzutti, F. Andreatta, M. Lekka, L. Fedrizzi, Microstructural and local electrochemical characterisation of Gr. 91 steel-welded joints as function of post-weld heat treatments. *Corrosion Sci.* **148**, 407–417 (2019). <https://doi.org/10.1016/j.corsci.2018.12.042>
- K. Li, J. Shan, C. Wang, Z. Tian, Effect of post-weld heat treatments on strength and toughness behavior of T-250 maraging steel welded by laser beam. *Mater. Sci. Eng. A* **663**, 157–165 (2016). <https://doi.org/10.1016/j.msea.2016.03.082>
- A. Sharma, D.K. Verma, S. Kumaran, Effect of post weld heat treatment on microstructure and mechanical properties of Hot Wire GTA welded joints of SA213 T91 steel. *Mater. Today: Proc.* **5**, 8049–8056 (2018). <https://doi.org/10.1016/j.matpr.2017.11.490>
- H.K.D.H. Bhadeshia, A.R. Chintia, Critical assessment 41: the strength of undeformed pearlite. *Mater. Sci. Technol.* **38**(16), 1291–1299 (2022). <https://doi.org/10.1080/02670836.2022.2079295>
- G. Mandal, S.K. Ghosh, S. Chatterjee, Effects of TMCP and QT on microstructure and properties of ultrahigh strength steel. *Mater. Today: Proc.* **18**, 5196–5201 (2019)
- G. Mandal, N.K. Tewary, S.K. Ghosh, Enhancement of mechanical properties in bainitic steel processed from different austenitization temperatures. *Steel Res. Int.* **89**(2), 1700259 (2018)
- G. Mandal, S.K. Ghosh, S. Bera, S. Mukherjee, Effect of partial and full austenitisation on microstructure and mechanical properties of quenching and partitioning steel. *Mater. Sci. Eng. A* **676**, 56–64 (2016)
- S. Dewangan, V.V. Nemade, K.H. Nemade, Critical analysis of material behaviour in welded plates of AISI 0.2%-C steel under as-welded, quenched and annealed conditions. *Acta Metall. Slovaca* **29**(1), 26–33 (2023). <https://doi.org/10.36547/ams.29.1.1719>
- The Welding Institute: <https://www.twi-global.com/technical-knowledge/faqs/faq-what-is-meant-by-postweld-heat-treatment-stress-relief-heat-treatment> (date of access: 21/02/2024)
- P. Moore, G. Booth, 13 - Improving the fracture performance and fatigue life of welded joints, Editor(s): Philippa Moore, Geoff Booth, *The Welding Engineer's Guide to Fracture and Fatigue*, Woodhead Publishing, (2015), Pages 185–195, ISBN 9781782423706, <https://doi.org/10.1533/9781782423911.2.185>.
- D. N. Croft, Chapter 3 - Effects of heat treatment, Editor(s): D N Croft, In *Woodhead Publishing Series in Welding and*

Other Joining Technologies, Heat Treatment of Welded Steel Structures, Woodhead Publishing, (1996), Pages 21–47, ISBN 9781855730168, <https://doi.org/10.1533/9781845698812.21>.

30. N.T. Nguyen, M.A. Wahab, The effect of undercut and residual stresses on fatigue behaviour of misaligned butt joints. *Eng. Fract. Mech. Fract. Mech.* **55**(3), 453–469 (1996)

Springer Nature or its licensor (e.g. a society or other partner) holds exclusive rights to this article under a publishing agreement with the author(s) or other rightsholder(s); author self-archiving of the accepted manuscript version of this article is solely governed by the terms of such publishing agreement and applicable law.

Publisher's Note Springer Nature remains neutral with regard to jurisdictional claims in published maps and institutional affiliations.